

Article

Pusher Propeller Performance Investigation on Lightweight Medium Range UAV

Agus Suprianto^{1,a}, Firman Hartono^{2,b}, Dana Herdiana^{1,c}, Deasy Tresnoningrum^{1,d,*}, and Nurhadi Pramana^{1,e}

¹ Research Center for Aeronautics Technology, Research Organization for Aeronautics and Space, National Research and Innovation Agency, Bogor, 16350, Indonesia

² Aerospace Engineering Study Program, Faculty of Mechanical and Aerospace Engineering, Bandung Institute of Technology, Bandung, 40132, Indonesia

E-mail: ^aagus137@brin.go.id, ^bfirman.hartono@itb.ac.id, ^cdana006@brin.go.id,

^{d,*}deas002@brin.go.id (Corresponding Author), ^enurh030@brin.go.id

Abstract. Research has been conducted to investigate the efficacy of a pusher-type propeller on a Lightweight Medium-Range UAV aircraft using two methods: Computational Fluid Dynamics (CFD) simulation and experimentation. Since there is a fuselage at the front, the performance of the propeller on this UAV aircraft may experience interference, making it necessary to investigate. This investigation aims to determine the difference in thrust coefficient (C_T), power coefficient (C_P), and efficiency (η) between the performance of the propeller with and without the fuselage, as well as the aerodynamic efficiency (L/D) of the propeller. The testing and simulation will have two configurations: propeller with the fuselage (power-off and power-on) and propeller without the fuselage (power off and power on). According to the results, putting the propeller behind the fuselage would decrease C_T and C_P at the same advanced ratio point as the configuration without a fuselage. At the same advanced ratio position, the propeller efficiency of the configuration with fuselage drops by approximately 5%. The comparison of simulation results with experiments shows the same pattern. Speed changes do not significantly affect aerodynamic efficiency (L/D). Propeller rotation (power on) significantly affects the aerodynamic efficiency (C_L/C_D) by an average of approximately 82-87%.

Keywords: Lightweight medium-range UAV, pusher-type propeller configuration, airframe interaction with propellers, computational fluid dynamics.

ENGINEERING JOURNAL Volume 28 Issue 9

Received 25 August 2023

Accepted 3 September 2024

Published 30 September 2024

Online at <https://engj.org/>

DOI:10.4186/ej.2024.28.9.11

1. Introduction

Studying the flight performance of the aircraft is crucial in the field of unmanned aerial vehicles (UAVs), especially for technology that can be utilized in surveillance and reconnaissance missions. The type of configuration model under study for the UAV is the pusher type. The pusher-type configuration design offers various advantages such as an unobstructed cockpit view due to the propulsion engine's positioning, which creates available space for electronic components including cameras. The design can also decrease vibrations or noise in the front cabin of the aircraft [1]. Furthermore, the distorted effect of fluid flow due to fuselage obstruction results in reduced propeller efficiency and thrust value [2].

Unmanned aircraft technology has been classified into two main categories: parameters based on take-off weight and range. Each category has different flight characteristics that depend on the flight mission [3]. This research highlights the selection of UAV technology studies in the medium-range category with a light take-off weight, which greatly affects speed during flight, particularly in the cruise phase, ceiling, climb rate, and maneuverability. Thus, it is necessary to comprehend the concept of flight characteristics of lightweight UAVs [4].

This research was preceded by Power-Off testing in a wind tunnel to determine the aerodynamic characteristics of an airplane without a propeller propulsion system. The main concern is to conduct a numerical computation (CFD) Power-On simulation study that models an airplane using a pusher-type propeller system; however, this test requires a larger capital budget compared to tests without a propeller propulsion system. Research is being conducted on the simulation of this configuration model because its effect is very intense, particularly on the back of the wing, but also extends forward with changes in the upwash angle [5]. Therefore, it is necessary to validate the simulation modeling, which requires experimental testing.

2. Methodology

2.1. Related Works

One of the main academic references for this research is an experiment conducted by [6] that measured the performance of the propeller without a fuselage. In addition, the propeller is rotated by a Scorpion SII-3032-990 kV brushless motor that is controlled by a Castle Creation ICE-75 Electronic Speed Controller (ESC), which is programmed to adjust the rotational speed (RPM) of the propeller. The electrical power source is provided by the ET-system LAB/SMS 435. The thrust and torque are measured using ATI Mini45 6 load cell components. During the load cell measurement, the frequency is about 1000 Hz, which provides an average value of approximately 2 seconds for the data logger.

Another significant academic reference for this study is an experiment conducted by [7], which examines the fuselage diameter to propeller diameter ratio with a value

range of 0.4 to 0.7. This also varies the chord width and thickness in the propeller geometry against the propeller diameter with a value range of 0.1 to 0.14. Tests were performed in a wind tunnel with wind speed specifications of approximately 50 m/s while varying propeller RPM rotation between 4500 to 6500 RPM.

2.2. Problem Definition

This paper examines how the performance of a pusher-type propeller is affected by the interaction with or without an aircraft fuselage. It also compares the propeller analysis results under conditions with or without the blockage effect caused by the fuselage during the numerical computational simulation (CFD) method. It is vital to validate the CFD method modeling with the Power-On configuration to yield a graphical trend that is relatively similar to the one obtained in the experimental method. This similarity is particularly important in measuring the thrust and torque moments and value of the thrust coefficient (C_T), power coefficient (C_P), and efficiency of the propeller model (η) under conditions with or without the fuselage blockage effect. Finally, this study aims to determine the changes in lift coefficient (C_L) and drag coefficient (C_D) of the fuselage model with or without a propeller by analyzing the numerical simulation results of the validated CFD method.

Experimental investigations of propeller dynamics have been conducted by varying engine speed (RPM) using a throttle regulator to obtain different thrust values at different speeds [8]. Similarly, researchers have investigated propeller aerodynamic parameters, especially for small-sized UAVs, through various methods, including experimentation with wind tunnels and CFD [9]. Experimental modeling investigations were carried out based on previous studies specifically isolated propeller models were tested with a diameter of 0.3 m to 0.4 m to adjust to the limited size of the wind tunnel used for testing [10-12]. The objective was to analyze the interaction of upstream and downstream fluid flow. Moreover, comparative tests were performed on non-dimensional propeller performance variables based on the effect of the Reynold number [13].

2.3. Theory

The theoretical foundation for examining the aerodynamic features of propellers is based on the combination of momentum and blade elements initially presented by Rankine and Froude [14]. Rankine's principle describes how to forecast the effectiveness that a propeller can achieve in specific working conditions while taking into account air velocities far ahead and behind the propeller that produce fluid pressure changes at the propeller rotation region [15]. Furthermore, given that this principle did not specify the required shape of the propeller for producing the desired thrust, Froude reduced the momentum equation to a two-dimensional airfoil view that overlooked both the three-dimensional

aspect ratio shape and vortex flow. Furthermore, a more modern theory was developed by merging these two classical principles. Glauert [16] formulated it by foreseeing slip in a vortex flow, employing a rigid, cylinder-shaped wake model, whereas Goldstein modeled periodic slip current in each part of the propeller airfoil utilizing circulation changes. However, the shortcoming of Goldstein's principle is the incapacity to scrutinize aerodynamic loads at small advance ratios [17].

Moreover, Theodorsen updated the theory by utilizing experimental and computational studies to improve the visualization of the fluid flow dynamics occurring through the propeller [18]. To determine the propeller performance's aerodynamic characteristics, the design parameters are calculated using a combination of three pre-existing theories, namely momentum theory, blade elements, and vortices, concisely formulated by Larrabee [19]. Analyzing the interaction between the airframe and the propeller requires non-dimensional variables to investigate the vortex wave flow area and the propeller's performance characteristics [20-21]. Similarly, Jeong-Hyun Cho's research analyzes the effects of Power-On on the pusher propeller type UAV by utilizing the following mathematical equations [22]:

$$C_T = \frac{T}{\rho N^2 D^4} \quad (1)$$

$$C_P = \frac{P}{\rho N^3 D^5} \quad (2)$$

$$P = \pi N Q \quad (3)$$

$$\eta = \frac{C_T}{C_P} J \quad (4)$$

$$J = \frac{v_\infty}{ND} \quad (5)$$

where J is non-dimensional units of advance ratio calculated based on freestream velocity, N is propeller rotational speed per minute (RPM), D is propeller diameter (m), P is propeller shaft power (SHP), T is propeller thrust (Newton), Q is propeller torque (Nm) and ρ is air density (kg/m^3).

Meanwhile, to estimate the amount of aerodynamic force on the pusher propeller as an interaction with the fuselage is formulated as :

$$C_D = \frac{F_Y}{\rho N^2 D^4} \quad (6)$$

$$C_L = \frac{F_Z}{\rho N^2 D^4} \quad (7)$$

$$C_D^* = \frac{D^*}{\frac{1}{2} \rho v^2 S} \quad (8)$$

$$C_L^* = \frac{L^*}{\frac{1}{2} \rho v^2 S} \quad (9)$$

C_D and C_L are non-dimensional units of drag and lift coefficients. C_D and C_L in Eq. (6) and (7) here mean drag and lift coefficients correlated to the force that works on the pusher propeller (that are F_Y for drag and F_Z for lift). While C_D^* and C_L^* are drag and lift coefficients correlated to the force that works on the pusher propeller with the fuselage. So the D^* and L^* are drag and lift (Newton), v is the velocity (m/s) and S is an area (m^2). The use of the * marks in Eq. (8) and (9) is intended to facilitate the distinction between the drag and lift working on a specific body of the aircraft (in this case, the pusher propeller with fuselage) and the drag and lift working on the aircraft as a whole.

The axial velocity of the freestream towards the propeller rotating plane significantly decreases due to fluid flow distortion, resulting in an imbalance in the loading on rotation, and causing strain on the propeller. This increase in loading causes the angle of attack to increase, which results in a subsequent increase in thrust and absorbed power. An increase in thrust may lead to a decrease in propulsion efficiency depending on propeller operating conditions. When influenced by fuselage interference, local speed will produce peak propulsion efficiency values at different advance ratio positions [23]. The blockage effect depends on the ratio of the largest fuselage diameter to the propeller diameter, which can be expressed by the following equation:

$$B = \frac{D_{fuselage}}{D_{propeller}} \quad (10)$$

According to [24], the blockage effect can be disregarded if the ratio value is below the critical value, which is approximately between 0.2 and 0.35. The interval value can be seen in Fig. 1 below :

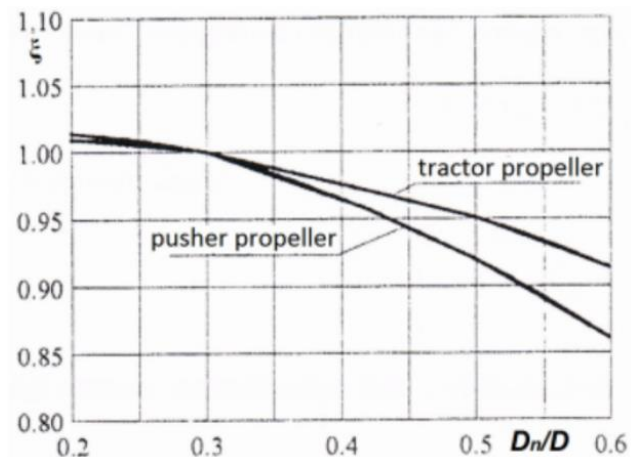


Fig. 1. Correction factor for pusher and tractor propeller types, based on the ratio of nacelle diameter to propeller diameter [25].

3. Experimental Setup and Computational Simulation

The model that was used in experimental testing refers to the unmanned aerial vehicle (PUNA) Alap-Alap BPPT and serves as a reference for making the test model. The test model is adjusted according to the size of the wind tunnel test section owned by Faculty of Mechanical and Aerospace Bandung Institute of Technology (FTMD ITB), which measures 1 meter in length and 40 centimeters in width and height, as shown in Fig. 2. This wind tunnel can operate at speeds of around 72 kilometers per hour. The turbulence intensity of the wind tunnel according to [26] is less than 1 percent. These results were obtained from measurements of freestream velocities between 1 and 20 m/s.



Fig. 2. Close Loop Wind Tunnel Testing [27].

The propeller test was modeled using the reverse engineering method because PUNA Alap-Alap BPPT used the original 18-inch x 10-inch propeller. This size was the main limitation of the research problem, so the scaling method was used. A scale of 1:0.555 was used to produce a model propeller size of approximately 10 inches x 6 inches.

The reverse engineering process starts by replicating the original propeller using a negative mold and creating a new product made of carbon fiber. This new product can then be cut to extract a portion of the airfoil surface in each section. Cutting each section of the carbon fiber propeller blade is performed to obtain the airfoil geometry of each section. This allows for the creation of a 3D CAD model image. The chord length, thickness of the airfoil, and blade angle measurement are measured for each blade section. The 3D CAD drawing of the propeller geometry is scaled with a factor of 0.555 to produce a 3D CAD drawing of a 10x6-inch propeller. Figure 3. shows the comparison between the original propeller and the scaled carbon fiber propeller 10x6 inches model.



Fig. 3. Comparison between the original 18x10-inch propeller and the 1:0.555 scale carbon fiber propeller 10x6-inch model.

The test equipment used to conduct the experiment has three main load cells: one to measure thrust and two to measure the moment (torque). The load cell configuration is shown in the Fig. 4.

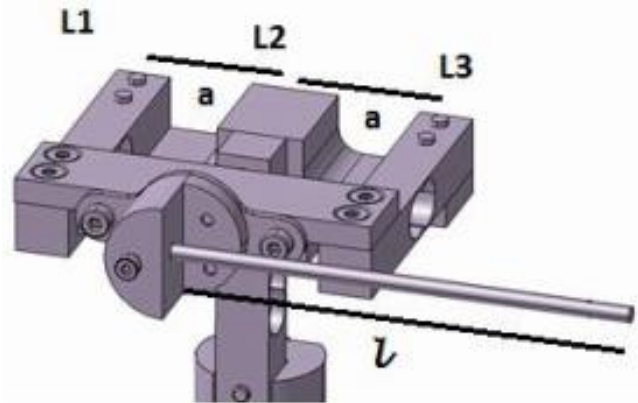


Fig. 4. Moment calibration rod and position of load cell on test bench test equipment [28].

Calibration is carried out using the calibration mode test equipment configuration. The load used to measure thrust is connected to the hanging pulley connecting rope, which is connected to the L2 load cell sensor. The load used to measure the moment (torque) is hung on the calibration rod, which is connected to the L1 and L3 load cell sensors.

The experimental testing of 10x6-inch model propeller was conducted in two stages. In the first stage, the propeller was tested without the fuselage included. Then in the second stage, the propeller was tested and attached to the fuselage which was configured in a pusher type with the propeller placed behind the aircraft fuselage. The experimental setup configuration is presented in Fig. 5.



Fig.5. Experimental setup configuration for testing without fuselage.

During each experimental stage of testing both without fuselage and with fuselage, one data sample was taken five times for uncertainty analysis. The dynamic testing was conducted at rotational speeds of 4000 RPM and 5000 RPM with corresponding airflow velocities of approximately 2.7 to 9.3 m/s for 4000 RPM and 3.3 to 10.9 m/s for 5000 RPM respectively.

The test data collection considers two primary parameters: the airflow velocity setting, which is only controlled through the potentiometer on the control board, and a passive force reading. This force will be utilized as a correction factor because the dynamic pressure generated is derived purely from the kinetic energy momentum of the wind tunnel fan rotation force.

A major consideration in determining the value of this correction factor is the presence of a propeller test piece with a cross-sectional area, A , and a test bench device inside the test section with a cross-sectional area, C . According to the Glauert correction [29], these areas can be calculated as follows:

$$\frac{v_{\infty}'}{v_{\infty}} = 1 - \frac{\tau\alpha}{2\sqrt{1+2\tau}} \quad (11)$$

$$\alpha = \frac{A}{C} \text{ and } \tau = \frac{T}{\rho A v_{\infty}^2} \quad (12)$$

$$J_{eff} = \frac{v_{\infty}'}{ND} \quad (13)$$

where A is an area of the propeller rotation (m^2), C is the cross-section area of wind tunnel test section (m^2), T is propeller thrust (Newton), v_{∞} is freestream velocity (m/s), v_{∞}' is corrected freestream velocity (m/s), ρ is air density (kg/m^3), N is propeller rotational speed per minute (RPM), D is propeller diameter (m), and J_{eff} is effective advance ratio calculated due to the effect of correction of the body area (fuselage) as a blockage (non-dimensional units).

In the case of measuring the correction factor with a configuration without a fuselage, the raw data of the measurement results read by the load cells L1 and L3 reveals a significant disparity between the test equipment installed with and without a propeller [28].

Test objects are modeled using numerical computing simulation (CFD). The simulated model is designed to be similar to the experimental modeling conditions so that this study undertakes two CFD models, namely propeller simulation modeling without a fuselage and propeller modeling with a fuselage, where the propeller is located at the back.

The fluid domain is defined as air using the ideal gas equation without the heat equation. The K-Omega Shear Stress Transport turbulent equation is used with a boundary layer thickness of approximately 0.5 mm based on calculations estimated from a reference that describes flat plate theory [30]. The computational domain model and boundary conditions for the propeller case, without the fuselage, are presented in Fig. 7.

General settings were used for the simulation as shown in Table 1.

Table 1. General settings for simulation.

Analysis type	Steady state
Stationary Domain	
Domain type	Fluid domain
Material	Air ideal gas
Morphology Option	Continuous fluid
Reference Pressure	101325 pa
Buoyancy Model	Non-buoyancy
Domain Motion	Stationary & Rotating
Angular Velocity	4000 RPM & 5000 RPM
Mesh Deformation Option	None
Heat Transfer Option	Isothermal
Fluid Temperature	25 °C
Turbulence Option	K-Omega Shear Stress Transport

To model the propeller only, it will be divided into nine sections along the span with illustration as shown in Fig. 6.



Fig. 6. Section division of the propeller along the span.

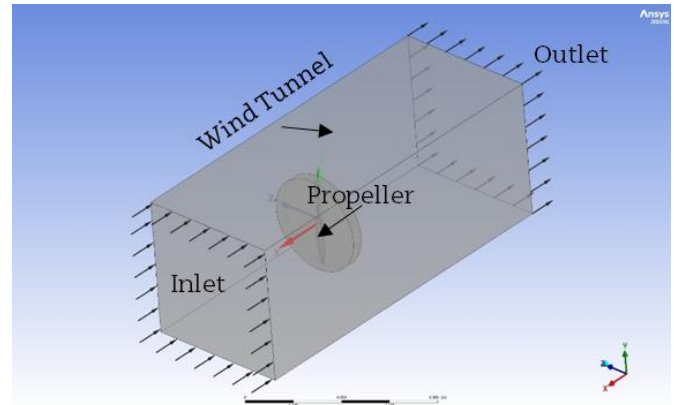


Fig. 7. Computational Domain Model and Boundary Conditions for propeller testing without fuselage.

The grid (mesh) selection process is performed using the Unstructured Mesh method by adding Inflation Program Controlled options to control detailed calculations, such as the thickness of the boundary layer (boundary thickness) and the number of layers in the boundary layer on each face defined before meshing, such as the testbench, propeller parts, and fuselage.

The parameters speed, pressure, RPM, and temperature will be used in this simulation. The speed variations used were 2.58 m/s, 4.41 m/s, 6.16 m/s, 7.51 m/s, and 9.28 m/s. Two RPM variations, 4000 and 5000, were used, with a pressure of 1 atm and a temperature of 25°C assumed.

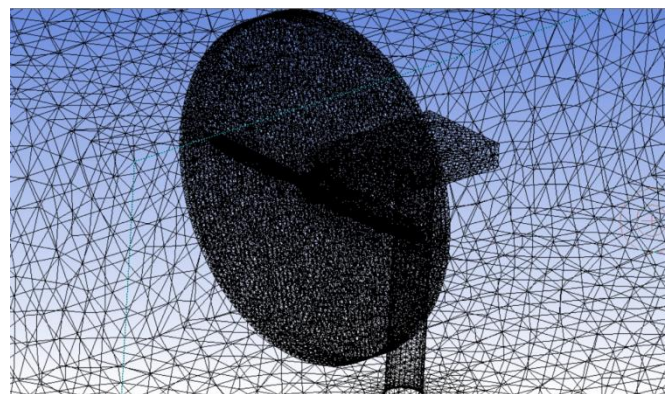


Fig. 8. Unstructured mesh CFD of 10x6 inches propeller without fuselage.

The model of the BPPT PUNA Alap-Alap Fuselage and Propeller Test Objects was performed using a scale of 1:0.555 from the original model, making it suitable to fit into the limited test section room, due to the limitations of the problem specified, namely only the effect of the interaction of the aircraft fuselage area on propeller

performance. Therefore, the model is made without the nose and main landing gear, twin booms, and ruddervators, and the length of the wing spans is reduced.

The Reynolds number of the BPPT Alap-Alap PUNA aircraft is approximately 3.732×10^5 at a cruise speed of 21 m/s or Mach number 0.06 [31]. However, scaling affects the Reynolds number, which results in its value changing to 6.904×10^4 at a flight speed of 7 m/s or Mach number 0.02. The flow conditions for this category remain under low subsonic, so the scaling effect can be safely confirmed to be negligible for the given aircraft.

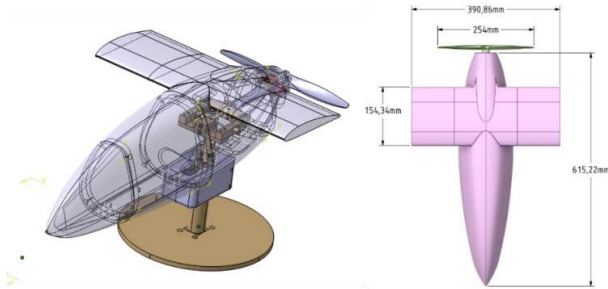


Fig. 9. 3D CAD Model of the experimental PUNA Alap-Alap BPPT fuselage, with a scale factor of 1:0.555.

The fuselage test objects are made from Acetal Thermoplastic material using a 3D printer measuring 20cm x 20cm x 60cm. The model is printed in 5 separate parts, which are then sanded, caulked, and painted as shown in Fig. 10.



Fig. 10. Model of the experimental PUNA Alap-Alap BPPT fuselage with a scale factor of 1:0.555 and experimental setup.

For CFD with fuselage modeling, all general settings and conditioning remain the same as in CFD without fuselage modeling.

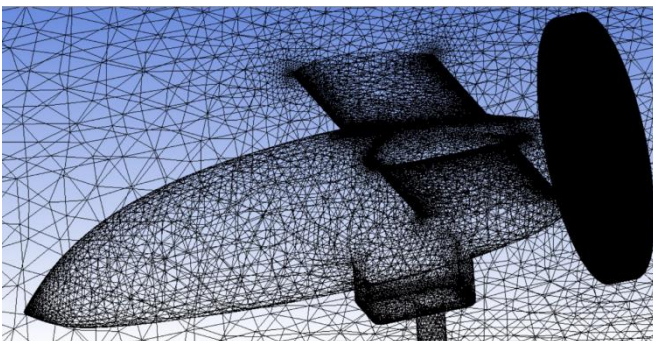


Fig. 11. Unstructured mesh CFD of 10x6 inches propeller configured behind fuselage.

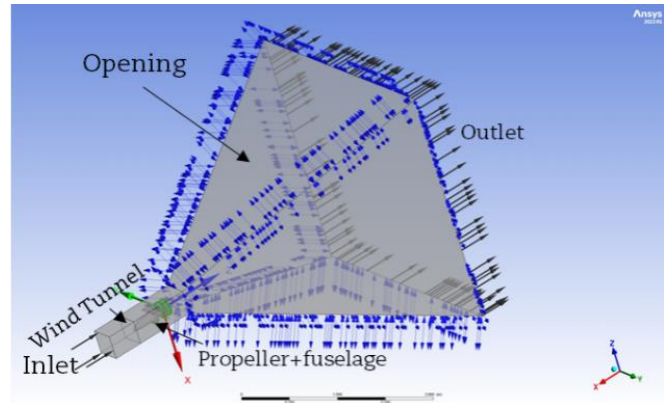


Fig. 12. Computational Domain Model and Boundary Conditions for propeller testing with fuselage.

The moving mesh technique was applied in order to rotate the propeller wall at a constant rotational speed and the K-Omega Shear Stress Transport (SST) turbulence model was used to model the turbulent features of the flow. Similarly, this is also applied to the surface of the fuselage model, where shear forces determine the speed profile along the fuselage. This method is a combination of the K-Epsilon and K-Omega models [32], it uses the K-Omega model near the wall and switches to a function of the K-Epsilon model when moving away from the wall closer to the upper limit of the boundary layer. The K-Omega SST model has been shown to give superior results for flows with strong adverse pressure gradients such as those appearing in the pusher propeller flow configuration [33], being able to describe the generation of specific vortices at the leading and trailing edges respectively.

To improve comparability between the settings for CFD pre-processing, Table 2 shows grid parameter identification for both configurations with and without fuselage.

Table 2. Grid Parameter Identification for CFD pre-processing

	Without Fuselage	With Fuselage
Face Size	$2.5 \times 10^{-4} - 2.5 \times 10^{-2}$	$5 \times 10^{-4} - 5 \times 10^{-2}$
Mesh Function	Curvature	
Relevance Center	Fine	
Mesh Quality :		
Element Quality	83 %	79.2 %
Skewness	22.4 %	23.3 %
Orthogonal Quality	77.3 %	76.5 %
Total Elements	9.151.926	9.342.158
Total Nodes	772.426	919.272

The discrete model has been tested to determine the number of elements that are required for accurate estimation of aerodynamic parameters such as axial, normal, and side force for aircraft wall body (see Fig. 13), and also thrust as axial force for propeller wall (see Fig. 14). For this purpose, a series of power on simulations were carried out, in which the mesh number of elements for each force divisions were changed.

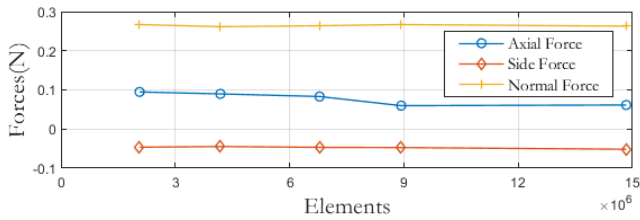


Fig. 13. Forces in axial (x-axis), side (y-axis), and normal (z-axis) for aircraft wall body.

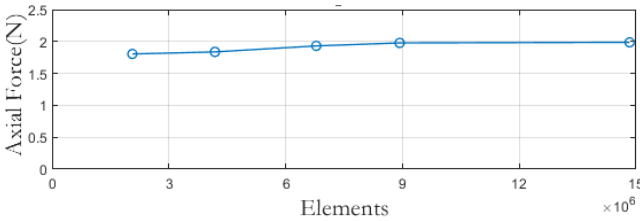


Fig. 14. Thrust as axial force for propeller wall.

According to that, for all cases in this work the number of 9 million grid elements was the same occurred during convergent simulation with different values, especially the aircraft axial force suddenly down from 0.1 into 0.06 Newton because of pressure and velocity distribution changes within propeller rotate increased from 1.75 into 2 Newton. The calculations also were carried out for normal and side force cases for the aircraft wall body. In this situation, the normal and side force on the aircraft wall body appears to be unaffected by the propeller torque, so the value of these forces seems like linear at 0.275 and -0.05 Newton throughout the change in its element value. An increase in the number of elements above 9 million does not cause a significant change in all of forces but leads to an increase in computational costs.

The mesh grid is in accordance with the independence study, however the number of meshes may still be insufficient due to inherent limitations in the use of computer simulations and the time consumption that involved. This may be a contributing factor to the discrepancy between experimental and CFD results.

4. Result and Analysis

Figure 15 presents a comparison for C_T between experimental test data and numerical computational simulation (CFD) data at 4000 RPM and 5000 RPM for both configurations.

Figure 15 and Fig. 16 compare CFD simulation data with experimental results for both configurations at 4000 RPM and 5000 RPM. The C_T thrust coefficient (see Fig. 15) for CFD is closer to the experimental results, while in the fuselage configuration, the C_T value for CFD is further away from the experimental results. This happens in the range of increasing advance ratio points. The interaction of the fuselage in front of the propeller may be responsible for the aerodynamic effect that increases the thrust value.

The CFD data for the power coefficient (C_P) (see Fig. 16) is shown to form a similar pattern both with and without the fuselage. This trend shows the estimated C_P

value getting closer to the experimental value, especially in the small advance ratio range of 0.10 to 0.40. However, as the advance ratio range goes above 0.40, the estimated C_P value moves away from the experimental value again. The decrease in the C_T value as the translational velocity increases may cause difficulty in modeling the flow release behind the propeller, leading to the mentioned issue.

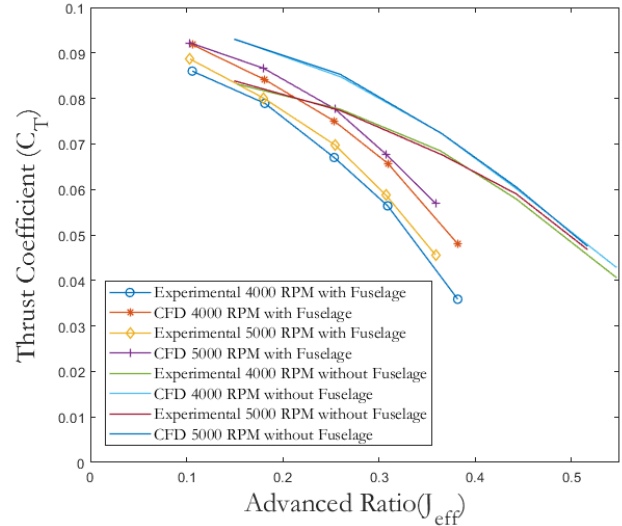


Fig. 15. Thrust Coefficient (C_T) with and without fuselage.

Figure 16 below shows the comparison of C_P for both configurations :

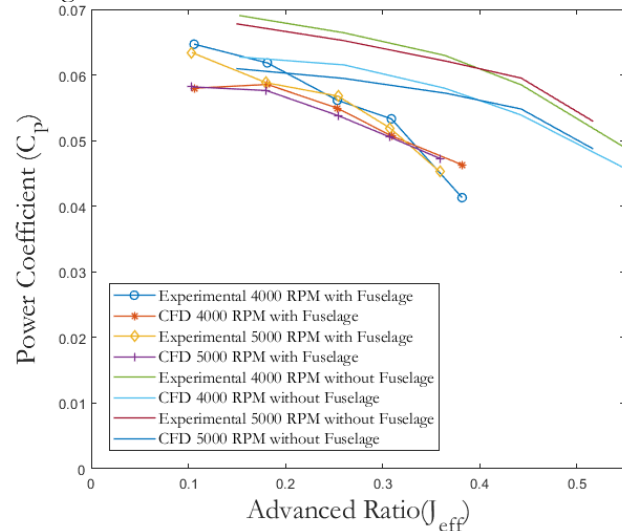


Fig. 16. Power Coefficient (C_P) with and without fuselage.

Figure 17 presents a comparison of dynamic efficiency (η) values between the results of CFD simulation data and experimental testing in both configurations, with and without the fuselage, at 4000 RPM and 5000 RPM.

As depicted in Fig. 17, the estimated efficiency values in the CFD data tend to deviate from the trend line of the test graph in both configurations, with and without the use of the fuselage. This observation indicates that the airflow area in front of the propeller (i.e., upstream) begins to be disturbed, so that the ratio of momentum energy generated from the propeller thrust force, C_T to its

absorption capability, C_p along the advance ratio also changes, characterized by the difference in error or deviation in each efficiency value which is around 16.3% at 4000 RPM and 16.4% at 5000 RPM for the uninstalled fuselage. Regarding the installed fuselage, there is a deviation of approximately 21.3% and 15.8% for each efficiency at 4000 RPM and 5000 RPM, respectively. Additional analysis indicates a reduction of approximately 5% in the peak efficiency value when utilizing the fuselage configuration across a wide range of advance ratios.

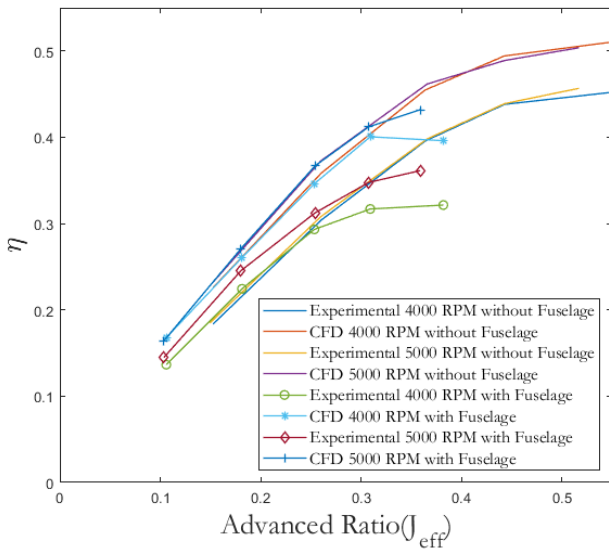


Fig. 17. Propeller efficiency with and without fuselage.

Additional research is conducted through an analysis of the aerodynamic efficiency parameters recorded as the ratio between lift and drag on each segment of the propeller airfoil profile with a configuration without fuselage, both in Power-Off (not rotated) and Power-On (rotated) conditions. Several key factors influence aerodynamic efficiency when operating the propeller in rotating or non-rotating conditions. The factors include blade pitch, propeller RPM, air velocity surrounding the propeller, as well as the type, shape, length, and number of blades. In Power-On conditions, the propeller provides thrust by rotating the blades. The movement of air through the propeller blades is inferred as the forward motion of the aircraft. This, in turn, creates distinct pressures moving between the front (upstream) and back (downstream) of the blades. This difference creates an aerodynamic force in the form of thrust, enabling movement forward relative to the torque force generated by the blade RPM rotation [34]. The thrust generated in these conditions is necessary to conquer air resistance (drag) and maintain an aircraft's speed.

In the Power-Off condition, where the propeller does not rotate, it is presumed that the engine is off. Thus, there is no direct thrust generated by the propeller. Typically, the primary thrust in this scenario is generated from the momentum obtained before shutting down the engine or from the plane's airspeed while descending. Because the propeller does not produce any thrust, the aerodynamic forces generated solely depend on the lift and drag

distribution throughout the spanwise propeller's airfoil profile [34].

Table 3. Variation of coefficient error and efficiency values errors for each test condition.

Fuselage Uninstalled						Fuselage Installed					
4000 RPM			5000 RPM			4000 RPM			5000 RPM		
ΔC_r	ΔC_F	$\Delta \eta$	ΔC_r	ΔC_F	$\Delta \eta$	ΔC_r	ΔC_F	$\Delta \eta$	ΔC_r	ΔC_F	$\Delta \eta$
0,117	-0,09	0,23	0,109	-0,1	0,233	0,068	-0,1	0,229	0,04	-0,08	0,134
0,092	-0,07	0,179	0,103	-0,09	0,21	0,066	-0,05	0,161	0,082	-0,02	0,104
0,058	-0,08	0,15	0,068	-0,08	0,16	0,12	-0,02	0,18	0,113	-0,05	0,174
0,039	-0,08	0,128	0,026	-0,08	0,114	0,166	-0,05	0,264	0,154	-0,03	0,185
0,055	-0,07	0,129	0,015	-0,08	0,103	0,339	0,121	0,232	0,248	0,044	0,195

Figure 18 and Fig. 19 are a comparison of the distribution of aerodynamic efficiency (L/D) values along the spanwise propeller's (r/R position) obtained from numerical computing (CFD) simulations of the propeller - one with rotation (Power-On), and the other without rotation (Power-Off) - under operational flight speeds ranging from 2.56 m/s to 9.28 m/s.

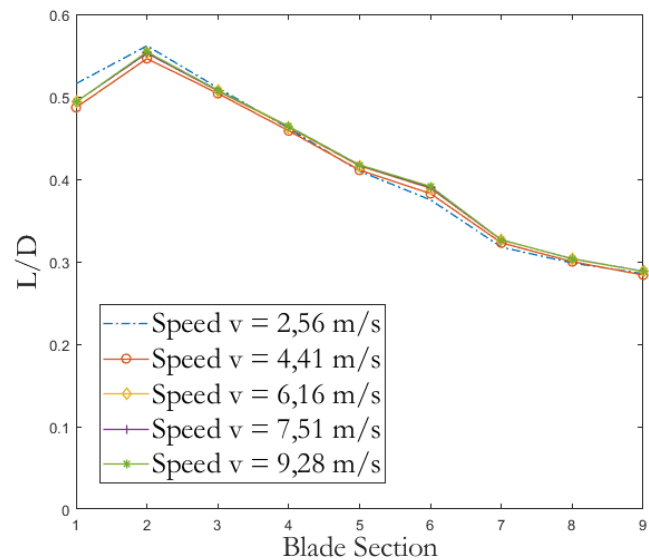


Fig. 18. Comparison of aerodynamic efficiency (L/D) data from CFD with flight speed variation for Power-Off propeller configuration without fuselage along the spanwise propeller (r/R position).

Figure 18 shows that the aerodynamic efficiency value peaks around 20% spanwise propeller with a maximum value (L/D) of about 0.55. Additionally, the given speed variation tends to produce relatively the same value. This condition is feasible because the axial velocity around the propeller becomes very low and it is not in a rotated condition (Power-Off). As a result, the outer radii of the propeller blades tends to have a lower L/D than the inner radii of the propeller because the airflow on the outside is more affected by the tip effect which causes aerodynamic resistance to increase.

Blades that are rotated or in Power-On conditions also have been studied. As shown in Fig. 19, the peak level of aerodynamic efficiency (L/D) increased by approximately 1.58% when the propeller was not rotated. Specifically, at 4000 RPM, the magnitude of L/D

increased to 1.42, while at 5000 RPM, the magnitude increased to 1.73 or 2.14% at a speed of 9.28 m/s. Furthermore, as shown in Fig. 18, the peak value of efficiency (L/D) shifts from a position of approximately 20% spanwise to a position of around 70% spanwise. This is because the airstream approaching the propeller blades has a higher axial velocity, caused by the influence of the tangential velocity resulting from the propeller's RPM rotation, which reduces the significance of the tip effect and decreases the L/D difference between the inner radii and outer radii of the propeller blades.

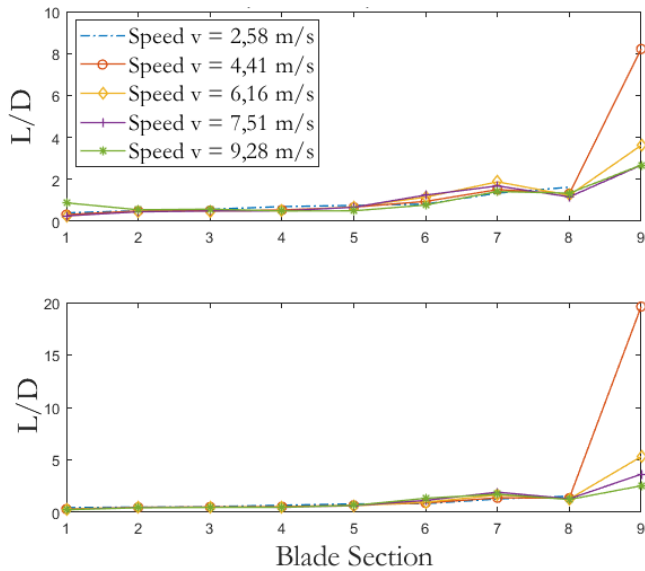


Fig. 19. Comparison of aerodynamic efficiency (L/D) data from CFD with flight speed variation for Power-On 4000 RPM (upper subplot) dan 5000 RPM (lower subplot) propeller configuration without fuselage along the spanwise propeller (r/R position).

Figure 20 compares the numerical computational data (CFD) for the distribution of aerodynamic efficiency of the propeller, considering the spanwise propeller (r/R position), during Power-Off and Power-On conditions at 4000 and 5000 RPM without fuselage. Furthermore, Fig. 21 shows the comparison of the aerodynamic efficiency of the propeller against Advanced Ratio (J_{eff}), without fuselage, for Power-Off and Power-On conditions at 4000 RPM and 5000 RPM.

Figure 20 simulation results of numerical computation (CFD) suggest that the aerodynamic lift and drag ratios per section of the airfoil blade from position 1 ($r/R = 10\%$) to position 5 ($r/R = 50\%$), while rotating at 4000 RPM and 5000 RPM, exhibit similar L/D efficiency values compared to the non-rotating state. L/D ratio values tend to decrease for 4000 RPM and increase for RPM 5000 rotations.

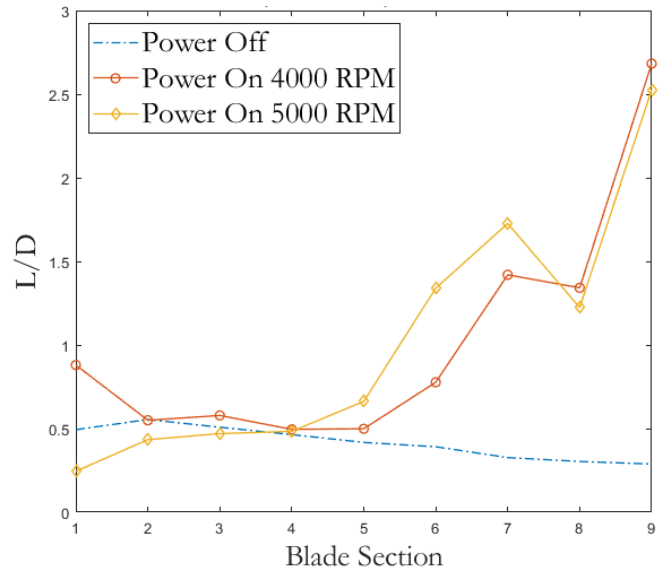


Fig. 20. Comparison of aerodynamic efficiency data for each spanwise propeller at axial velocity 9.28 m/s under Power-Off and Power-On conditions.

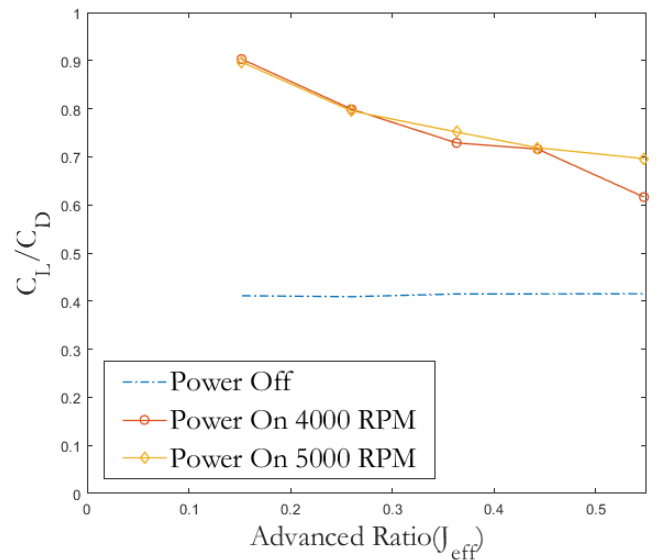


Fig. 21. Comparison of non-dimensional aerodynamic efficiency of propeller against advanced ratio under Power-Off and Power-On conditions.

The cause for such changes in Fig. 20 is the difference in values of propeller forward rate ratio or advance ratio, despite the axial velocity around the propeller being constant at 9.28 m/s. Referring to Fig. 17, the propeller's dynamic efficiency (without a fuselage configuration) remains nearly the same for 4000 RPM and 5000 RPM with values of 0.45 and 0.44 respectively, whereas the corresponding propeller forward rotation rates produced by the advance ratio values for these RPMs are 0.55 and 0.44 respectively. These results suggest that rotation at 4000 RPM results in a bigger lift distribution with lower drag, however, a decrease in the angle of attack at the airfoil blade section leads to a lower L/D value.

On the other hand, at 5000 RPM, the absorbed power is higher when the propeller dynamic efficiency is lower, resulting in an increase in the L/D ratio. After moving from the position of the 6th blade airfoil section ($r/R =$

60%) to the 9th ($r / R = 90\%$), the L/D efficiency tends to increase almost equally at both RPM revolutions up to the point of the 7th blade airfoil section ($r / R = 70\%$) because the rotational speed increases, along with changes in the blade section's angle of attack, which has started to reduce towards the tip of the propeller.

Furthermore, Fig. 21 shows the distribution of non-dimensional aerodynamic efficiency coefficients in propeller RPM rotations of 4000 and 5000 (Power-On) and without rotation (Power-Off), which are more general in nature, without considering the influence of the magnitude of the aerodynamic forces involved or the influence of the environment. The values of efficiency (C_L/C_D) reduced in all three parameters as the advance ratio increased. The values of non-dimensional aerodynamic efficiency (C_L/C_D) of the propeller rotating at 4000 RPM and 5000 RPM, with an axial velocity of 9.28 m/s, are 0.62 and 0.69, respectively, at point 0.55 of the same advance ratio, while at point 0.44 both are equal to 0.72. This indicates that the rate of efficiency reduction

with respect to the addition of advance ratio is around 4.3% more effective at 5000 RPM than at 4000 RPM, where it is only 16.1%.

Analyzing aerodynamic interactions of fluid flow phenomena in front of and behind the propeller, the CFD post-processing results are presented in Fig. 22 - Fig. 25.

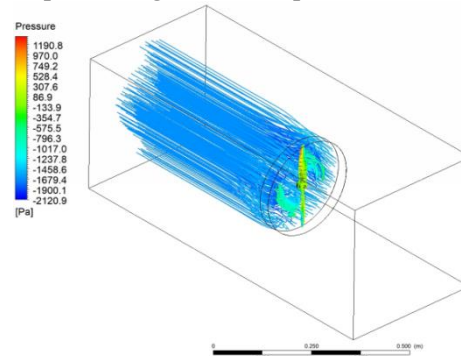


Fig. 22. Pressure contour at 9,28 m/s without fuselage [35].

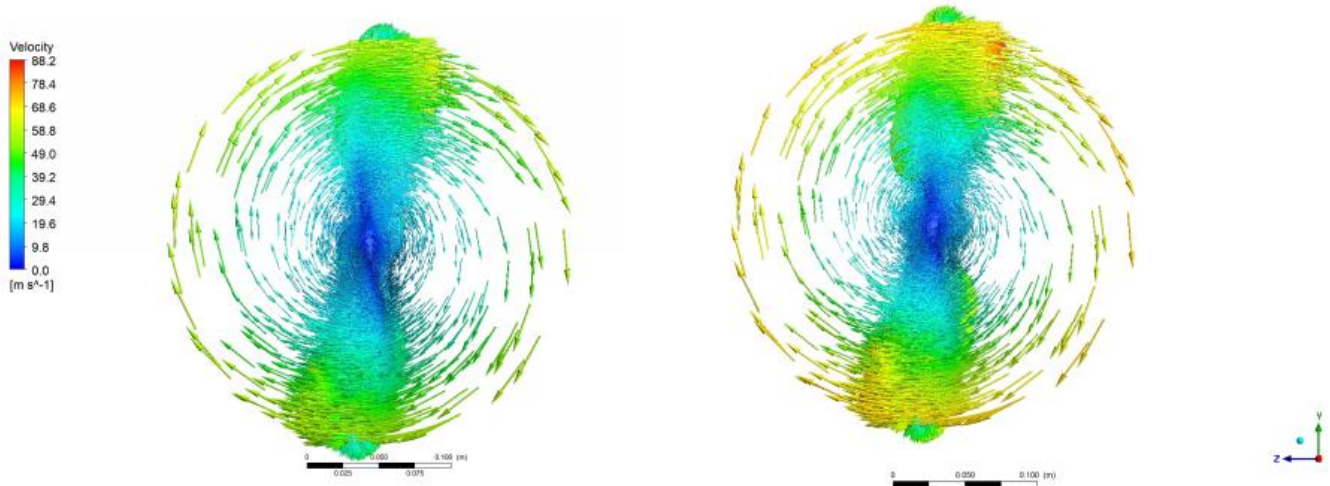


Fig. 23. Velocity contour at 9,28 m/s on 4000 and 5000 RPM without fuselage [35].

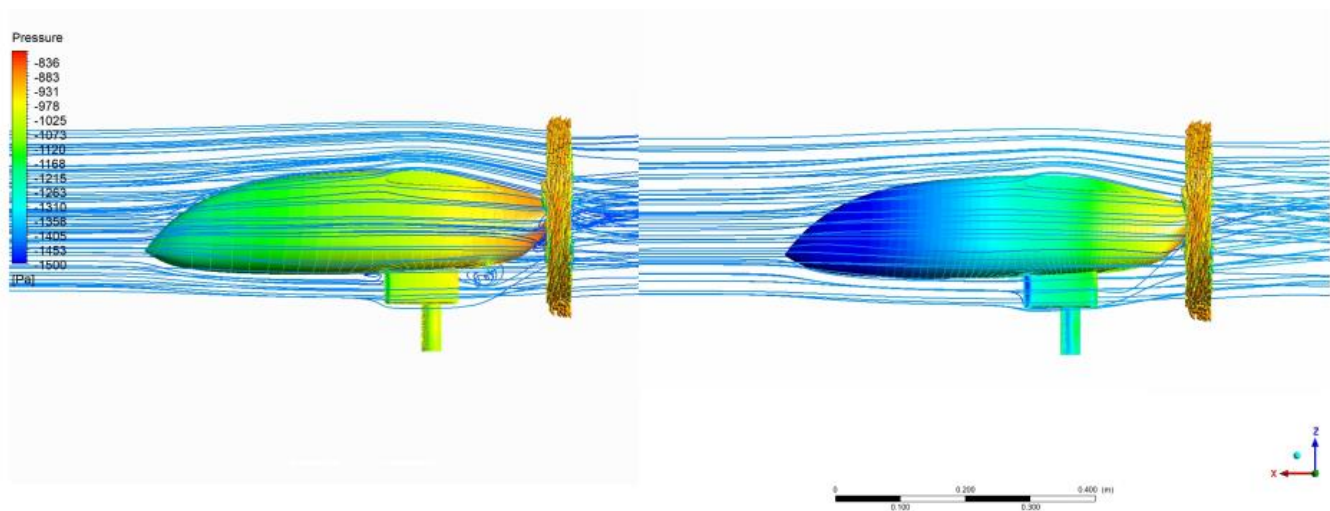


Fig. 24. Pressure contour at 9,28 m/s on 4000 and 5000 RPM with fuselage [35].

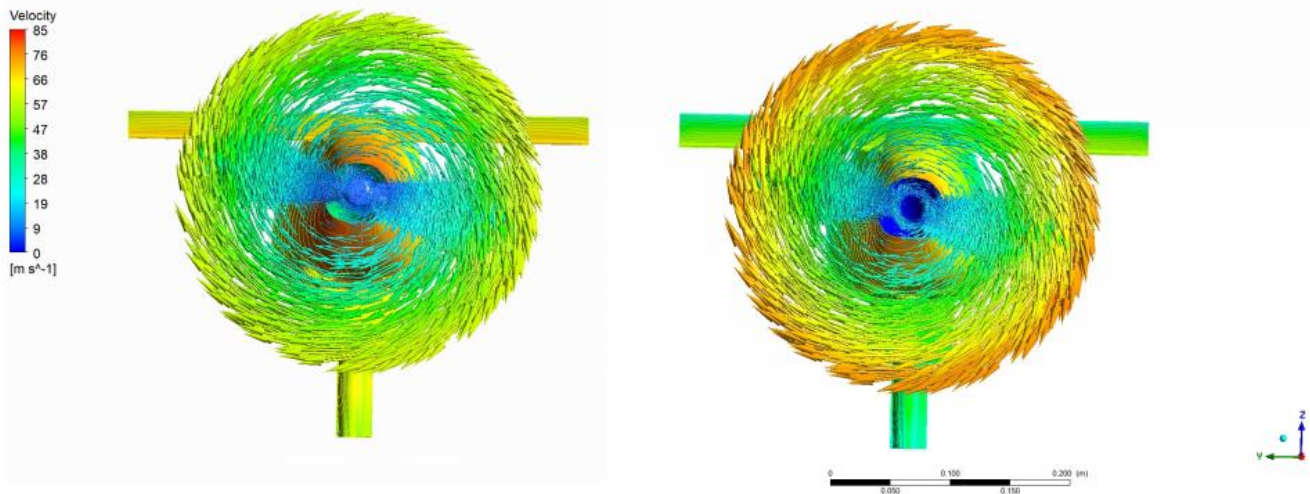


Fig. 25. Velocity contour at 9,28 m/s on 4000 and 5000 RPM with fuselage [35].

Figures 22-25 depict the flow visualization under three configurations with different RPM and contours, for a flow velocity of 9.28 m/s. Figure 22 shows the flow visualization for the propeller configuration only, without the fuselage, in the Power-Off condition. The figure also illustrates the pressure contour on the propeller, where red indicates high pressure, and blue indicates low pressure. The airflow passing through the propeller has not experienced turbulence, thus remaining streamlined. Figure 23 illustrates the flow visualization for the propeller configuration only, without the fuselage, in the Power-On condition. It shows the visualization of the airflow around the propeller, with the propeller being rotated at two settings: 4000 and 5000 RPM. For 4000 RPM, the propeller rotates in the clockwise direction, producing forward thrust. The speed generated by the propeller rotation is around 50-60 m/s. For 5000 RPM, with the same direction of rotation as 4000 RPM, the propeller rotational speed is around 60-70 m/s. Figure 24 depicts the flow visualization for the propeller configuration with the fuselage, in the Power-On condition. As seen in both Fig. 24 and 25, the airflow passing through the fuselage remains straight. However, when entering the propeller rotation, the flow becomes loose, forming a vortex (slipstream). At both 4000 and 5000 RPM, the flow velocity produced by the rotation of the propeller decreased in the propeller configuration with the fuselage, as a result of the interaction between the propeller and the resistance of the fuselage.

The hypothesis that can be derived from this phenomenon is that simulating propeller rotation (Power-On) in the presence of a fuselage can increase the kinetic energy, thereby accelerating the fluid flow passing through the surface of the fuselage. Consequently, the dynamic pressure also increases, while the rotational speed decreases. Additionally, the control volume of the fluid flow (streamline) is observed to be more regular when a fuselage is present in front of the propeller, compared to the scenario without a fuselage. This occurrence is beneficial since the fluid flow over the surface of the fuselage appears to receive some energy that helps

maintain the flow separation just before it reaches the propeller boundary [36].

5. Conclusions

After analyzing the obtained results, we draw the following conclusions :

- 1) The ratio of the largest diameter of the fuselage to the diameter of the propeller in this test needs to be studied, given that the ratio value of 0.6 has already been shown to have an effect of blockage on the performance of the propeller under test.
- 2) The wind speed correction factor generated in the wind tunnel test section proves to be very appropriate for configurations with and without a fuselage, as it can already provide the results of differences in C_T and C_P values along the advanced ratio, J , at the same point. Here, a drop in the propeller efficiency value of around 5% is noted.
- 3) Other parameters related to the effect of aerodynamic interaction on propeller performance can also be analyzed through CFD simulation. In the case of fuselage simulation with propeller rotation or Power-On simulation, the lift and drag values tend to be higher than in fuselage simulation without propeller rotation or Power-Off simulation.
- 4) The comparison between numerical computation (CFD) simulations and experimental test values shows good agreement when viewed from the C_T and C_P graph trends. However, it needs to be studied in detail regarding modeling, particularly the separation of fluid flow behind the propeller (for configurations without fuselage) and in front of the propeller (for configurations with fuselage).
- 5) Changes in speed have no significant effect on aerodynamic efficiency (L/D).
- 6) Propeller rotation (Power-On) has a significant impact on the aerodynamic efficiency (C_L/C_D), averaging about 82-87%.

Acknowledgment

This research was funded by The Agency for The Assessment and Application of Technology (BPPT). The funding covers scholarships, the cost of research equipment, and fees for international academic presentations.

Statement Of Author

All Authors in this paper and research are Main Contributors.

References

- [1] P. Ruchala, "An influence of pusher propeller cover on its performance – a concept of wind tunnel investigation," *Journal of KONES Powertrain and Transport*, vol. 23, no. 4, 2016. [Online]. Available: <https://www.semanticscholar.org/paper/An-influence-of-pusher-propellercover-on-its-%3A-a-Rucha%C5%82a/18af36855833ddb0daba2a21195e712234b8317a>
- [2] G. Snorri, "The anatomy of the propeller," in *General Aviation Aircraft Design Applied Methods and Procedures*, 1st ed. USA: Butterworth-Heinemann; Elsevier, 2014.
- [3] Z. Oksana and M. Alexandra, "Classification of UAV (Unmanned Aerial Vehicle)," unpublished student abstract, 2023 [Online]. Available: http://read.meil.pw.pl/abstracts/StudentAbstract_Zakora_Molodchik.pdf [Accessed: 01 July 2023].
- [4] U.S. Department of Transportation, Federal Aviation Administration, Pilot's Handbook of Aeronautical Knowledge, 2023. Available: https://www.faa.gov/regulations_policies/handbooks_manuals/aviation/faa-h-8083-25c.pdf. [Accessed: July 5, 2023].
- [5] K. Chinwicharnam and C. Thipyopas, "Comparison of wing-propeller interaction in tractor and pusher configuration," *International Journal of Micro Air Vehicles*, vol. 8, no. 1, pp. 3-20, 2016. [Online]. Available: <https://journals.sagepub.com/doi/10.1177/1756829316638206>.
- [6] D. Verstraete and R. MacNeill, "The effect of blockage on the performance of small propeller," presented at *20th Australasian Fluid Mechanics Conference*, Perth, Australia, 5-8 December 2016.
- [7] G. V. Vitaly, and P. V. Olga, and P. V. Albert, "Aerodynamic interference optimization of the fuselage-pushing propeller configuration," presented at *11th International Conference on Mechanical and Aerospace Engineering*, 2020. [Online]. Available: <https://www.semanticscholar.org/paper/Aerodynamic-Interference-Optimization-of-the-Gubskiy-Pavlenko/acdbccfd1e10ecf5c14b51cef22cece38753dad5>
- [8] R. K. Tripathi, V. Tiwari, I. Khunger, and P. Berwal, "Development of propeller test rig and evaluation of propeller performance," *International Research Journal of Engineering and Technology (IRJET)*, vol. 2, no. 8, pp. 1161-1167, Nov. 2015.
- [9] X. Liu, D. Zhao, and N. L. Oo, "Comparison studies on aerodynamic performance of a rotating propeller for small-size UAVs," *Aerospace Science and Technology*, vo. 133, p. 108148, 2023. [Online]. Available: <https://doi.org/10.1016/j.ast.2023.108148>
- [10] N. Van Arnhem, R. de Vries, T. Sinnige, R. Vos, G. Eitelberg, and L. L. Veldhuis, "Engineering method to estimate the blade loading of propellers in nonuniform Flow," *ALAA Journal*, vol. 58, no. 12, pp. 5332-5346, 2020. [Online]. Available: <https://doi.org/10.2514/1.J059485>
- [11] Q. Li, K. Öztürk, T. Sinnige, D. Ragni, G. Eitelberg, L. L. Veldhuis, and W. Yangang, "Design and experimental validation of swirl-recovery vanes for propeller propulsion systems," *ALAA Journal*, vol. 56, no. 12, pp. 4719-4729, 2018. [Online]. Available: <https://doi.org/10.2514/1.J057113>
- [12] N. Van Arnhem, R. Vos, and L. L. Veldhuis, "Aerodynamic loads on an aft-mounted propeller induced by the wing wake," in *Proceedings of the ALAA Scitech 2019 Forum*, San Diego, CA, USA, 7–11 January 2019. [Online]. Available: <https://arc.aiaa.org/doi/book/10.2514/MSCITECH.H19>
- [13] R. W. Deters, G. K. Ananda Krishnan, and M. S. Selig, "Reynolds number effects on the performance of small-scale propellers," in *Proceedings of the 32nd ALAA Applied Aerodynamics Conference*, Atlanta, GA, USA, 6–20 June 2014. [Online]. Available: <https://www.semanticscholar.org/paper/Reynolds-number-effects-on-the-performance-of-Deters-Krishnan/c218bd9bb4f08d4a4884bb0161fe1dbe8deca187>
- [14] W. M. J. Rankine and R.E. Froude, "On the Mechanical principles of the action of the propeller," *Transaction of the Institute of Naval Architects*, no. 6, pp. 13-39, 1889.
- [15] T. Von Karman, *From Low Speed Aerodynamic to Astronautics—International Series of Monographs in Aeronautics and Astronautics*. Institute for Fluid Dynamics and Applied Mathematics, University of Maryland: McGraw-Hill Education, 1963, no. 40, pp. 75-78.
- [16] H. Glauert, "Airplane propellers," in *Aerodynamic Theory*. W. F. Durand, Ed. New York: Springer, vol. IV, division, L, pp. 169-360, 1935. [Online]. Available: http://dx.doi.org/10.1007/978-3-642-91487-4_3
- [17] S. Goldstein, "On the vortex theory of screw propellers," *Proc. Roy. Soc. London, Ser. A, Math., Phys., Eng. Sci.*, vol. 123, no. 792, pp. 440–465, Apr. 1929. [Online]. Available:

- <https://royalsocietypublishing.org/doi/10.1098/rspa.1929.0078>
- [18] T. Theodorsen, *Theory of Propellers*. McGraw-Hill, 1948.
- [19] E. Larrabee, "Practical design of minimum induced loss propellers," *SAE International*, vol. 88, pp. 2053-2062, 1979. [Online]. Available: <https://www.jstor.org/stable/44699041>
- [20] R. M. A. Marretta, G. Davi, G. Lombardi, and A. Milazzo, "Hybrid numerical technique for evaluating wing aerodynamic loading with propeller interference," *Computers & Fluids*, vol. 28, pp. 923-950, 1999. [Online]. Available: [https://doi.org/10.1016/S0045-7930\(98\)00055-3](https://doi.org/10.1016/S0045-7930(98)00055-3)
- [21] G. K. Politis, "Simulation of unsteady motion of a propeller in a fluid including free wake modeling," *Engineering Analysis with Boundary Elements*, vol. 28, pp. 633-653, 2004. [Online]. Available: <https://doi.org/10.1016/j.enganabound.2003.10.004>
- [22] J. Hyun Cho, "Experimental and numerical investigation of the power-on effect for a propeller-driven UAV," *Aerospace Science and Technology*, vol. 36, pp. 55-63, July 2014. [Online]. Available: <https://doi.org/10.1016/j.ast.2014.04.001>
- [23] B. Jones, *Elements of Practical Aerodynamic*, 3rd ed. New York, John Wiley & Sons, 1942.
- [24] F. E. Weick, "Full-scale wind tunnel test with a series of propellers of difference diameters on a single fuselage," National Advisory Committee for Aeronautics, NACA-TP-339, 1931.
- [25] Z. Klepacki and P. Strzelczyk, „Uniwersalne charakterystyki śmigła,” *Prace Instytutu Lotnictwa*, vol. 1, no. 152, pp. 61-68, 1998.
- [26] Z. Bramantasaputra, "Characterizing wind tunnel turbulence statistics using hotwire anemometer," undergraduate thesis, FTMD, ITB, Bandung, West Java, 2022.
- [27] Institut Teknologi Bandung, "Wind Tunnel, Aset Berharga Pengembangan Kedirgantaraan di ITB," Institut Teknologi Bandung, 2020. [Online]. Available: <https://www.itb.ac.id/news/read/5184/home/win>
- d-tunnel-aset-berharga-pengembangan-kedirgantaraan-di-itb
- [28] Z. S. Islami and F. Hartono, "Development of small propeller test bench system," *The International Conference on Aerospace and Aviation, IOP Conf. Series: Materials Science and Engineering*, vol. 645, p. 012017, October 2019. [Online]. Available: [doi:10.1088/1757-899X/645/1/012017](https://doi.org/10.1088/1757-899X/645/1/012017)
- [29] H. Glauert, "Wind tunnel interference on wings, bodies and aircrews," *Aeronautical Research Committee Research and Memoranda*, no. 1566, Sep 1933. [Online]. Available: <https://apps.dtic.mil/sti/pdfs/ADA953012.pdf>
- [30] E. F. Jaguaribe, "The flat plate boundary layer equation under Blasius restrictions with a unique solution," *Mathematical Problems in Engineering*, vol. 2022, no. 1, p. 9032974, 2022.
- [31] The Agency for the Assessment and Application of Technology, "Design organization," Technical Document no. D013PA6000, Indonesia, 2017.
- [32] F. R. Menter, "Two-equation Eddy-viscosity turbulence models for engineering applications," *ALAA J.*, vol. 32, pp. 269-289, Aug. 1994. [Online]. Available: <https://doi.org/10.2514/3.12149>
- [33] J. Yin, A. Stuermer, and M. Aversano, "Aerodynamic and aeroacoustic analysis of installed pusher-propeller aircraft configurations," *Journal of Aircraft*, vol. 49, no. 5, pp. 1423-1433, 2012. [Online]. Available: <https://doi.org/10.2514/1.C031704>
- [34] J. Unnikrishnan, S. Ambadi, and P. Ghughthyal, "Performance analysis of a small-scale master airscrew propeller using experimental and analytical methods," *International Research Journal of Engineering and Technology (IRJET)*, vol. 7, no. 6, Jun. 2020.
- [35] ANSYS, *Software Package V 23.0*, 2023.
- [36] M. Figat and P. Piątkowska, "Numerical investigation of mutual interaction between a pusher propeller and a fuselage," *Proceedings of the Institution of Mechanical Engineers, Part G: Journal of Aerospace Engineering*, vol. 235, no. 1, pp.40-53, 2020. [Online]. Available: <https://doi.org/10.1177/0954410020932796>



Agus Suprianto was born in Jakarta, Indonesia, in 1986. In 2010, he received a Bachelor's degree in aeronautical engineering with a concentration in propulsion from Air Marshal Suryadarma University, East Jakarta, and in 2019, he received a Master's degree in aerospace engineering with a concentration in aerodynamic propulsion from Bandung Institute of Technology, Bandung.

He worked at BPPT from 2011 to 2021, and the institution later changed to BRIN. He has been working at BRIN since 2021. He conducts research in the fields of aerodynamics, propulsion design, and the performance of UAVs. His research interests include aerodynamics and propulsion simulation or experiments, the design of high-altitude propellers, the programming of aircraft performance, and the conceptual design of electric aircraft.



Firman Hartono was born in Cirebon, Indonesia, in 1977. He is an assistant professor in the Faculty of Mechanical and Aerospace Engineering at Bandung Institute of Technology (ITB) in Indonesia. He has been a member of the Aircraft Design, Operation, and Maintenance (ADOM) research group since 2008. In 2007, he earned his doctorate in propulsion from ITB. He also earned his Master's degree as well as his Bachelor's degree in 2002 and 2000, respectively, from ITB. His research mainly focuses on aircraft propulsion, particularly the aerodynamics of rotating machinery and combustion. He teaches aircraft propulsion, as well as instrumentation, measurement, experimentation, basic aerodynamics, and propulsion aerodynamics.



Dana Herdiana was born in Bandung, West Java, Indonesia in 1980. In 2004, he earned a Bachelor's degree in Aerospace Engineering from Nurtanio University in Bandung. Then, he received a Master's degree in Aerospace Engineering from the Bandung Institute of Technology in Bandung in 2021.

Between 2006 and 2021, he worked at LAPAN. The institution later changed to BRIN. Since 2021, he has been working at BRIN. He conducts research in the field of aerodynamics. Numerous journals and proceedings have published articles on aerodynamics. His research interests pertain to aerodynamics simulations and experiments, parachute design, downwash, slipstream, and aircraft performance. Additionally, he is a member of the Indonesian Research Association (PPI).



Deasy Tresnoningrum was born in Jakarta, Indonesia, in 1984. In 2007, she received a Bachelor's degree in astronomy, and in 2020, she obtained a Master's degree in aerospace engineering with a concentration in flight mechanics. Both of these degrees were earned from the Bandung Institute of Technology (ITB) located in Bandung, Indonesia.

Between 2008 and 2021, she worked at LAPAN, and the institution has since changed its name to BRIN. She has been working at BRIN since 2021. Her research work is focused on the flight dynamics of aircraft. Her research interests include aircraft performance, aircraft flight dynamics simulation and analysis, and conceptual design of aircraft. She is also a member of The Indonesian Research Association (PPI).



Nurhadi Pramana was born in Mataram, Indonesia, in 1990. In 2013, he earned his Bachelor's degree in aeronautical engineering with a specialization in structural design and analysis from ITB in West Java.

Between 2014 and 2021, he worked at BPPT, one of the national research agencies, in the Research Unit of Defence Industry. Since 2021, the agency has reformed into BRIN. His research work mainly focuses on the design and analysis of UAV structures. His research interests include manufacturing design, static analysis, fatigue analysis, and the exploration of composite materials.